Electronic Supplementary Material (ESI) for Energy & Environmental Science.
This journal is © The Royal Society of Chemistry 2024

A highly crystalline donor enables over 17% efficiency for small-molecule organic solar cell

Tao Zhang,[a, b] Cunbin An, *[a] Pengqing Bi, [a] Kaihu Xian,[c] Zhihao Chen,[a] Jingwen Wang, [a] Ye Xu, [a] Jiangbo Dai,[a, b] Lijiao Ma,[a] Guanlin Wang,[a, b] Xiaotao Hao, [d] Long Ye,[c] Shaoqing Zhang [a] and Jianhui Hou*[a, b]

[a]State Key Laboratory of Polymer Physics and Chemistry, Beijing National Laboratory for Molecular Sciences, Institute of Chemistry Chinese Academy of Sciences, Beijing 100190, China.

[b]University of Chinese Academy of Sciences, Beijing 100049, China.

[c]School of Materials Science & Engineering, Tianjin Key Laboratory of Molecular Optoelectronic Sciences, Tianjin University, and Collaborative Innovation Center of Chemical Science and Engineering, Tianjin 300350, China.

[d]School of Physics, State Key Laboratory of Crystal Materials, Shandong University, Jinan, Shandong 250100, P. R. China.

*E-mail: ancunbin@iccas.ac.cn; hjhzlz@iccas.ac.cn.

Instruments and Measurements

^{1}H NMR and ^{13}C NMR spectra were recorded in deuterated solvents on a Bruker DPX 300 or 400. Elemental analysis was performed on an instrument of Flash EA1112. Density functional theory (DFT) calculations were carried out using the level of B3LYP/6-31G(d,p). The UV-vis absorption spectroscopy measurements were conducted on a Hitachi UH4150 spectrophotometer. Differential scanning calorimetry (DSC) measurements were tested by DSC Q100 V9.0 Build 275 analyzer under purified nitrogen gas flow with a 10 ^{o}C / min heating rate. Electrochemical cyclic voltammetry measurements were performed on a CHI650D electrochemical workstation with a three-electrode system. Pt wire and glassy carbon electrode were used as the counter electrode and working electrode, respectively. Ag/Ag^{+} was used as the reference electrode, and the ferrocene/ferrocenium redox couple (Fc/Fc^{+}) was used as the internal calibration. Ultraviolet photoelectron spectroscopy (UPS) was measured by using Thermo Scientific ESCALAB 250Xi with a He-discharged lamp. The *J*–*V* measurements were performed by using the solar simulator (SS-F5-3A, Enlitech) along with AM 1.5G spectra (100 mW/cm^{2}). The EQE spectra were measured through the Solar Cell Spectral Response Measurement System QE-R3011 (Enli Technology Co., Ltd., Taiwan). The photoinduced charge extraction by linearly increasing voltage (photo-CELIV) measurements reported were performed by the all-in-one characterization platform Paios developed and commercialized by Fluxim AG, Switzerland. In order to reflect the true information, all of the organic solar cells (OSCs) are prepared for photo-CELIV measurements according to the corresponding device fabrication conditions. Ramp Rate: 0.10 V/us; Delay Time: 70 us; Light-Pulse Length: 30 us; Setup-Type: LED. Highly Sensitive EQE (*s*-EQE) was measured by using an integrated system (PECT-600, Enlitech), where the photocurrent was amplified and modulated by a lock-in instrument. Electroluminescence (EL) quantum efficiency (EQE_{EL}) measurements were performed by applying external voltage/current sources through the OSCs (ELCT-3010, Enlitech). AFM height and phase images were recorded on a Nanoscope AFM microscope (Bruker), where the tapping mode was used. The samples were fabricated in accordance with the conditions of the best OSCs. Grazing incidence wide-angle X-ray scattering (GIWAXS) measurements were performed on a Xeuss 2.0 SAXS/WAXS system (Xenocs SA, France). Cu Kα X-ray source (GeniX3D Cu ULD) generated at 50 kV and 0.6 mA and was utilized to produce X-ray radiation with a wavelength of 1.5418 Å. A semiconductor detector (Pilatus 300 K, DECTRIS, Swiss) with a resolution of 487×619 pixels was used to collect the scattering signals. The incident angle was 0.2°.

Transient absorption (TA) spectroscopy

Femtosecond transient absorption spectroscopy was measured on an Ultrafast Helios pump-probe system in collaboration with a regenerative amplified laser system from Coherent. An 800 nm pulse with a repetition rate of 1kHz, a length of 100 fs, and an energy of 7 mJ/pluse, was generated by a Ti:sapphire amplifier (Astrella, Coherent). Then the 800 nm pulse was separated into two parts by a beam splitter. One part was coupled into an optical parametric amplifier (TOPAS, Coherent) to generate the pump pulses at 400 and 800 nm. The other part was focused onto a sapphire plate and a YAG plate to generate white light supercontinuum as the probe beams with spectra covering 420-800 nm and 750-1600 nm, respectively. The time delay between the pump and probe was controlled by a motorized optical delay line with a maximum delay time of 8 ns. The sample films were spin-coated onto the 1 mm-thick quartz plates and encapsulated by epoxy resin in a nitrogen-filled glove box to resist water and oxygen in the air. The pump pulse is chopped by a mechanical chopper with 500 Hz and then focused on the mounted sample with probe beams. The probe beam was collimated and focused into a fiber-coupled multichannel spectrometer with CCD sensor. The energy of pump pulse was measured and calibrated by a power meter (PM400, Thorlabs).

Device fabrication

Fabrication of the OSCs via a spin-coating method. OSCs were fabricated with the conventional device structure (glass/ITO/PEDOT:PSS/active layers/PDINN/Ag). ITO-coated glass was purchased from South China Xiang's Science & Technical Company Limited. PEDOT:PSS (4083) was purchased from the Clevios^{TM}. BTP-eC9 and PDINN were purchased from Solarmer Material Inc. PEDOT:PSS was diluted with the same volume of water. PDINN was dissolved in methanol at the concentration of 1.5 mg/ml. B3TR: BTP-eC9 and B2: BTP-eC9 with weight ratio of 1:1 were dissolved in chloroform at the concentration of 20 mg/mL. The solutions of BTP-eC9 and B2: BTP-eC9 need to be stirred at 50˚C until completely dissolved. Both OSCs were fabricated by the following conditions: Firstly, about 10 nm PEDOT:PSS layers were spin-coated on the pre-cleaned ITO substrates and annealed at 150°C for 15 min. Subsequently, the substrates were transferred to the nitrogen glove box. The mixed solutions were spin-coated onto the PEDOT:PSS layers, and then the films were treated with chloroform solvent vapor annealing (SVA) 70s in a 60 mm diameter dish. The best active layer thickness is about 100 nm. PDINN was spin-coated on the top of the active layers at 3000 rpm for 30 s. Finally, 150 nm Ag was deposited under a high vacuum. The device contact area is 0.09 cm^2. The area of the mask is about 0.0617 cm^2.

Charge transport properties. The hole mobilities was measured by the SCLC method, employing a device architecture of ITO/PEDOT:PSS/ active layer/Au.

Synthetic detail:

5'',5''''-(4,8-bis(5-(2-ethylhexyl)thiophen-2-yl)benzo[1,2-b:4,5-b']dithiophene-2,6-diyl)bis(3',3''-dihexyl-[2,2':5',2''-terthiophene]-5-carbaldehyde) (S3)

Compound **S1** (0.905 g, 1 mmol), compound **S2** (1.205 g, 2.3 mmol) and $Pd(PPh_3)_4$ (57.8 mg, 0.05 mmol) were added into a 100 mL two-neck flask with 40 mL of dry toluene. The reaction mixture was refluxed overnight. The reaction mixture was filtered and the crude product was purified by silica gel column chromatography to give the product as yellow solid (1.29 g, 88%). ^{1}H NMR (400 MHz, $CDCl_3$), δ 9.87 (s, 2H), 7.70 (d, *J* = 8.0 Hz, 2H), 7.60 (s, 2H), 7.32 (d, *J* = 8.0 Hz, 2H), 7.22 (d, *J* = 8.0 Hz, 2H), 7.09 (s, 2H), 6.99 (s, 2H), 6.95 (d, *J* = 8.0 Hz, 2H), 2.92 (d, *J* = 8.0 Hz, 4H), 2.83 (m, 8H), 1.74–1.67 (m, 10H), 1.51–1.33 (m, 40H), 1.02-0.88 (m, 24H); ^{13}C NMR (100 MHz, $CDCl_3$) δ 182.52, 146.08, 146.06, 142.54, 142.19, 141.15, 138.72, 137.44, 137.37, 136.82, 136.80,136.01,135.57, 130.38, 129.50, 129.03, 128.38, 127.85, 125.84, 125.50, 123.38, 119.21, 41.52, 32.55, 31.66, 30.36, 30.22, 29.81, 29.68, 29.29, 29.27,28.99, 25.88, 23.08, 22.61, 14.23, 14.10, 14.08, 11.00. HRMS (MALDI, $C_{84}H_{102}O_2S_{10}$ m/z): calc. 1462.5081, found 1462.5075.

(5Z,5'Z)-5,5'-(((4,8-bis(5-(2-ethylhexyl)thiophen-2-yl)benzo[1,2-b:4,5-b']dithiophene-2,6-diyl)bis(3',3''-dihexyl-[2,2':5',2''-terthiophene]-5'',5-diyl))bis(methaneylylidene))bis(3-ethyl-2-thioxothiazolidin-4-one) (B3TR)

To the solution of compound S3 (400 mg, 0.273 mmol) in dry chloroform (40 mL) was added rhodamine S4 (435 mg, 2.7 mmol) followed by adding 0.2 mL of piperidine. The reaction mixture was refluxed overnight. The reaction mixture was filtered and the crude product was purified by silica gel column chromatography to give the product as red solid (397 mg, 83%). ^{1}H NMR (400 MHz,$CDCl_3$), δ 7.74 (s, 2H), 7.47 (2H), 7.30 (2H), 7.26 (2H), 7.24 (2H), 7.09 (2H), 6.96 (4H), 6.89 (2H), 4.15 (q, *J* = 4.0 Hz, *J* = 8.0 Hz, 4H), 2.95 (d, *J* = 8.0 Hz, 4H), 2.76 (m, 8H), 1.67 (br, 2H), 1.54 (br, 8H), 1.45 (br, 40H), 1.28 (br, 6H), 1.02-0.89 (m, 24H); ^{13}C NMR (100 MHz, $CDCl_3$) δ 191.84, 167.14, 145.82, 145.81, 144.34, 141.78, 140.73, 138.52, 137.20, 136.93, 136.80, 135.68, 135.30, 134.50, 130.51, 129.60, 128.71, 128.17, 127.88, 126.18, 125.43, 124.85, 123.11, 120.05,119.00, 41.54, 39.86, 34.43, 32.61, 31.75, 31.71, 30.22, 29.98, 29.85, 29.40, 29.02, 25.91, 23.12, 22.71, 22.67,14.26, 14.16, 12.28, 11.03. HRMS (MALDI, $C_{94}H_{112}O_2S_{14}$ m/z): calc. 1748.4808, found

1748.4795.

5',5'''-(4,4',8,8'-tetrakis(5-(2-ethylhexyl)thiophen-2-yl)-[2,2'-bibenzo[1,2-b:4,5-b']dithiophene]-6,6'-diyl)bis(3'-hexyl-[2,2'-bithiophene]-5-carbaldehyde) (S7)

Compound **S5** (1.0 g, 0.675 mmol), compound **S6** (0.555 g, 1.55 mmol) and $Pd(PPh_3)_4$ (39 mg, 0.03375 mmol) were added into a 100 mL two-neck flask with 40 mL of dry toluene. The reaction mixture was refluxed overnight. The reaction mixture was filtered and the crude product was purified by silica gel column chromatography to give the product as red solid (1.0 g, 87%). ^{1}H NMR (400 MHz,$CDCl_3$), δ 9.78 (s, 2H), 7.61 (d, *J* = 4.0 Hz, 2H), 7.51 (s, 2H), 7.46 (s, 2H), 7.30 (m, 4H), 7.10 (d, *J* = 4.0 Hz, 2H), 6.94 (d, *J* = 4.0 Hz, 2H), 2.95 (d, *J* = 8.0 Hz, 8H), 2.70 (m, 4H), 1.63 (m, 4H), 1.54–1.33 (br, 48H), 1.03-0.89 (m, 30H); ^{13}C NMR (100 MHz, $CDCl_3$) δ 182.25, 145.92, 145.87, 145.82, 142.80, 142.03, 138.82, 138.56, 137.62, 137.22, 137.12, 137.07, 136.85, 136.74, 136.61, 129.62, 128.21, 128.01, 127.82, 125.70, 125.43, 125.37, 123.44, 123.15, 120.79, 119.57, 41.45, 34.44, 32.63, 31.64, 30.05, 29.95, 29.35, 28.98, 25.83, 23.11, 23.09, 22.61, 14.22, 14.08, 11.01, 10.98. HRMS (MALDI, $C_{98}H_{114}O_2S_{12}$ m/z): calc. 1706.5457, found 1706.5463.

(5Z,5'Z)-5,5'-(((4,4',8,8'-tetrakis(5-(2-ethylhexyl)thiophen-2-yl)-[2,2'-bibenzo[1,2-b:4,5-b']dithiophene]-6,6'-diyl)bis(3'-hexyl-[2,2'-bithiophene]-5',5-diyl))bis(methaneylylidene))bis(3-ethyl-2-thioxothiazolidin-4-one)) (B2)

To the solution of compound S7 (400 mg, 0.234 mmol) in dry chloroform (40 mL) was added rhodamine 4 (377.3 mg, 2.34 mmol) followed by adding 0.2 mL of piperidine. The reaction mixture was refluxed overnight. The reaction mixture was filtered and the crude product was purified by silica gel column chromatography to give the product as red solid (383 mg, 82%).^{1}H NMR (400 MHz,$CDCl_3$), δ 7.52 (s, 2H), 7.24-7.18 (br, 8H), 7.07 (d, *J* = 8.0 Hz, 2H), 6.92 (br, 6H), 6.69 (s, 2H), 3.98 (d, *J* = 8.0 Hz, 4H), 2.98 (d, *J* = 8.0 Hz, 8H), 2.54 (br, 4H), 1.82 (br, 4H), 1.58–1.38 (br, 48H), 1.19-0.94 (m, 36H); ^{13}C NMR (100 MHz, $CDCl_3$) δ 191.64, 166.97, 145.55, 144.56, 142.02, 138.60, 138.35, 137.18, 137.10, 136.89, 136.67, 136.32, 134.40, 130.15, 128.15, 128.01, 125.80, 125.43, 124.69, 123.09, 122.86, 120.47,119.64, 119.33, 41.62, 41.61, 39.80, 34.66, 32.90, 31.91, 30.48, 30.05, 29.71, 29.20, 25.98, 23.33, 22.91, 14.45, 14.39, 12.39, 11.26, 11.18. HRMS (MALDI, $C_{108}H_{124}N_2O_2S_{16}$ m/z): calc. 1992.5189, found 1992.5179.

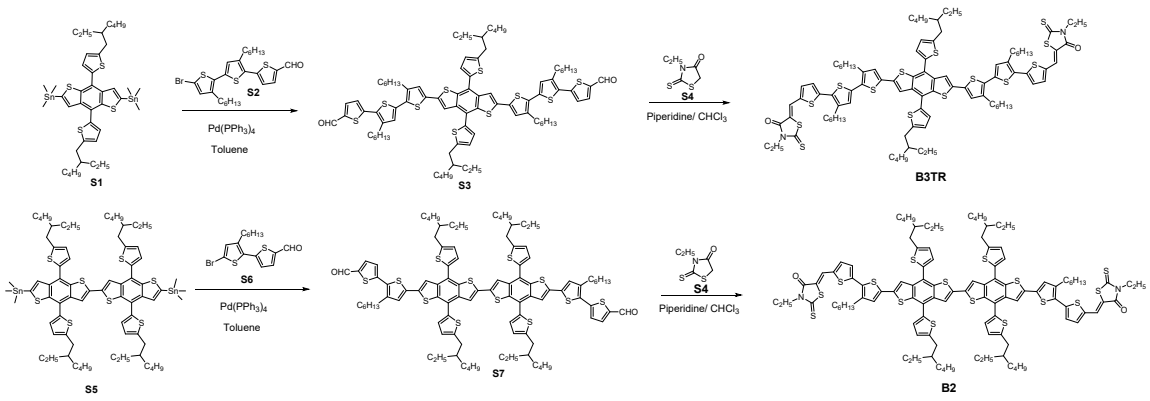

Scheme S1. The synthetic route of B3TR and B2.

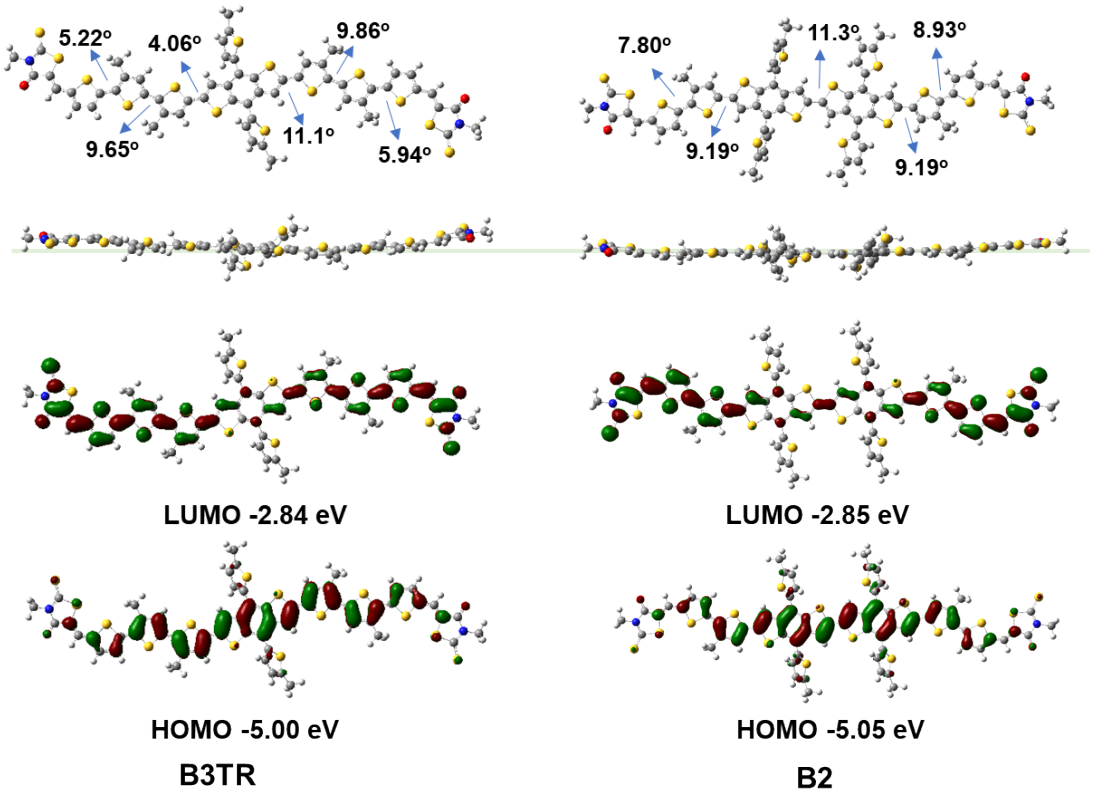

Figure S1. DFT (B3LYP, 6-31G (d,p)) calculated the model molecules of B3TR and B2.

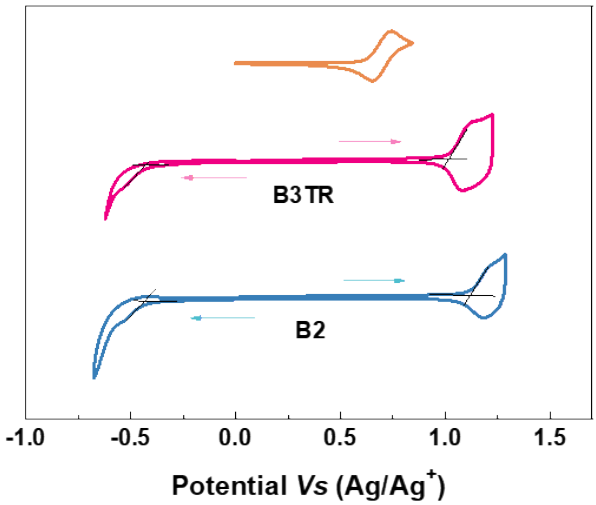

Figure S2. Electrochemical cyclic voltammetry curves of B3TR and B2.

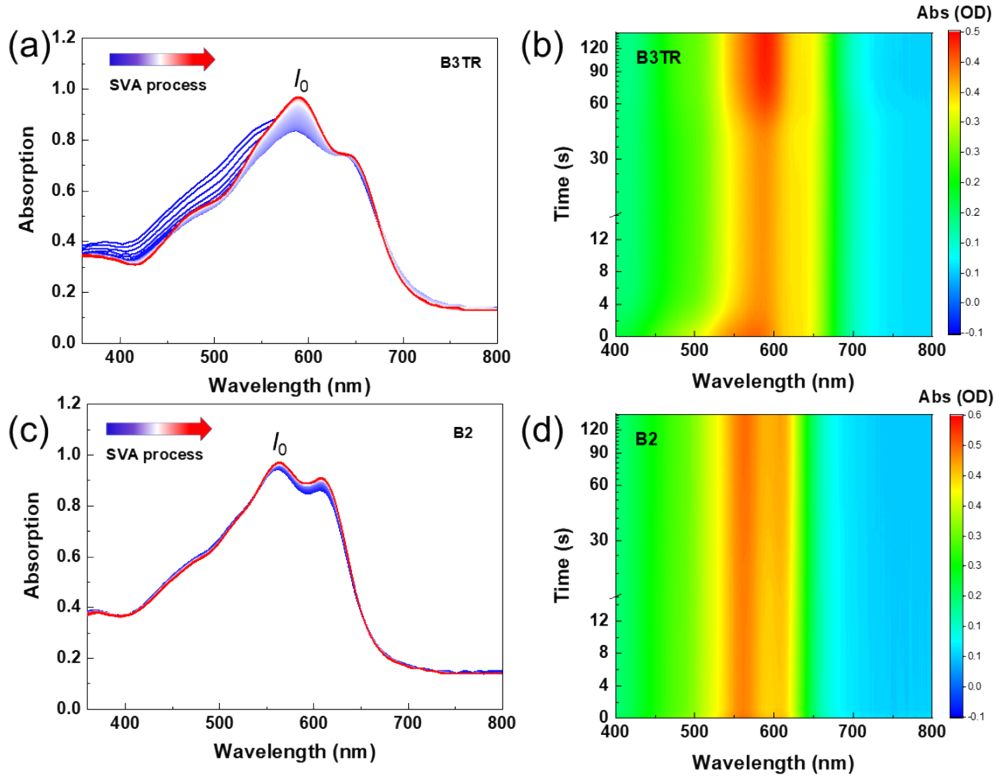

Figure S3. (a,c) In situ UV-visible absorption spectra and (b,d) in situ 2D UV-visible absorption profile of B3TR and B2 during CF SVA process.

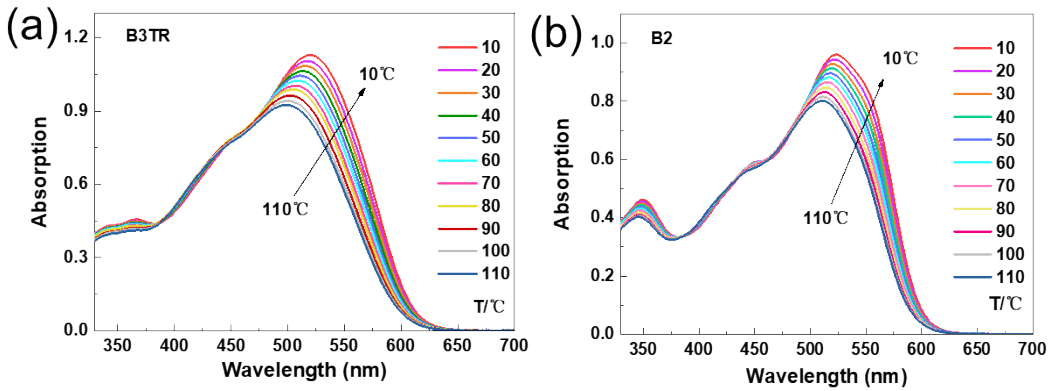

Figure S4. The temperature-dependent absorption spectra of (a) B3TR and (b) B2 in CB solution.

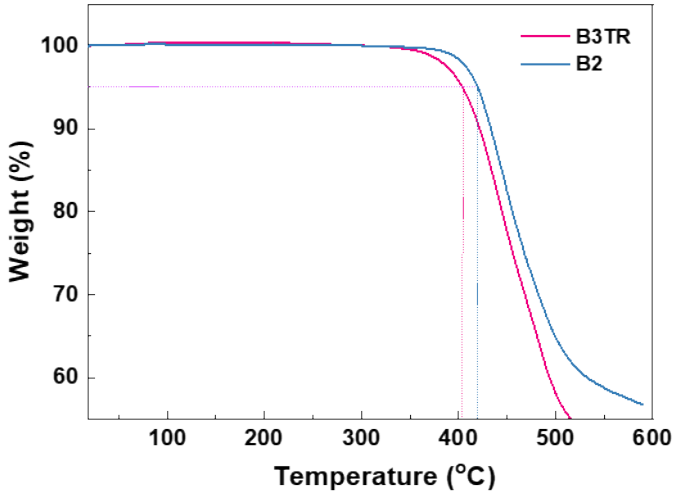

Figure S5. The TGA curves of B3TR and B2.

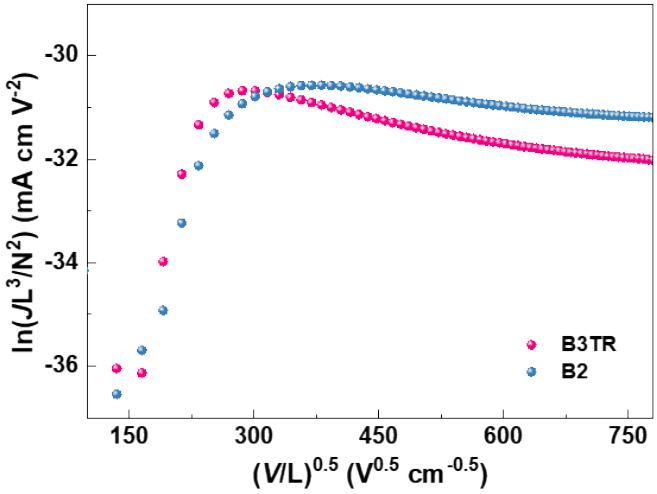

Figure S6. The hole mobilities of B3TR and B2.

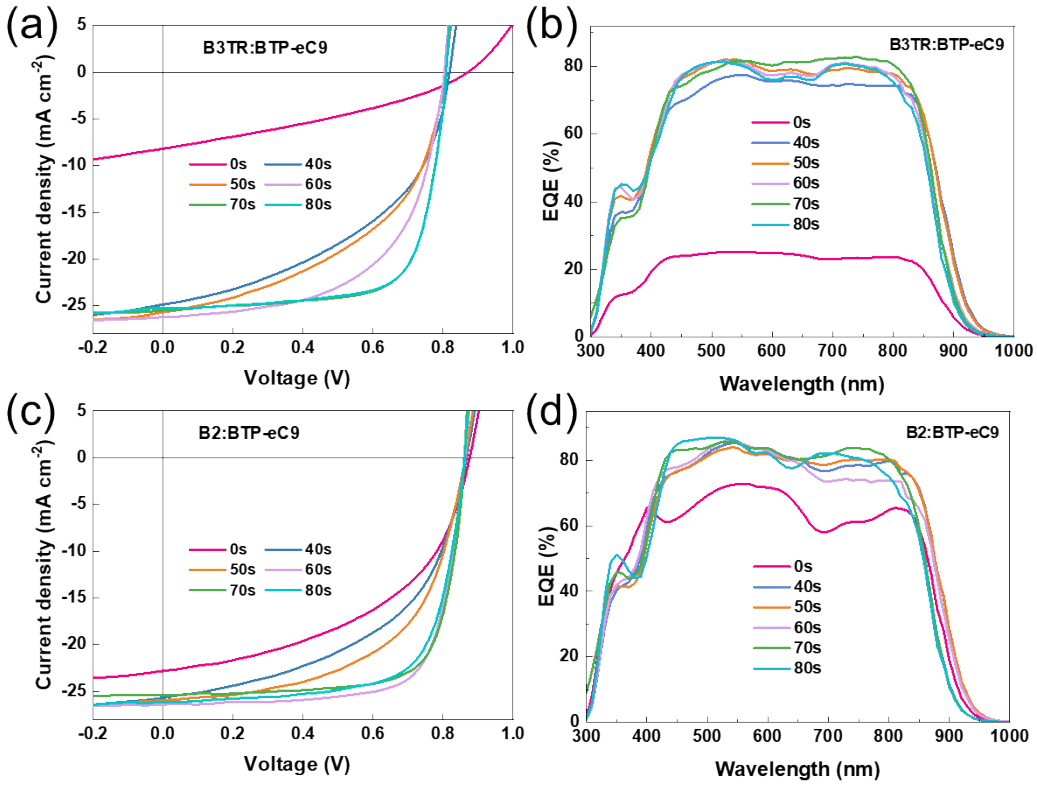

Figure S7. *J-V* and EQE curves of (a, b) B3TR:BTP-eC9- and (c, d) B3TR:BTP-eC9-based cells for different CF SVA duration.

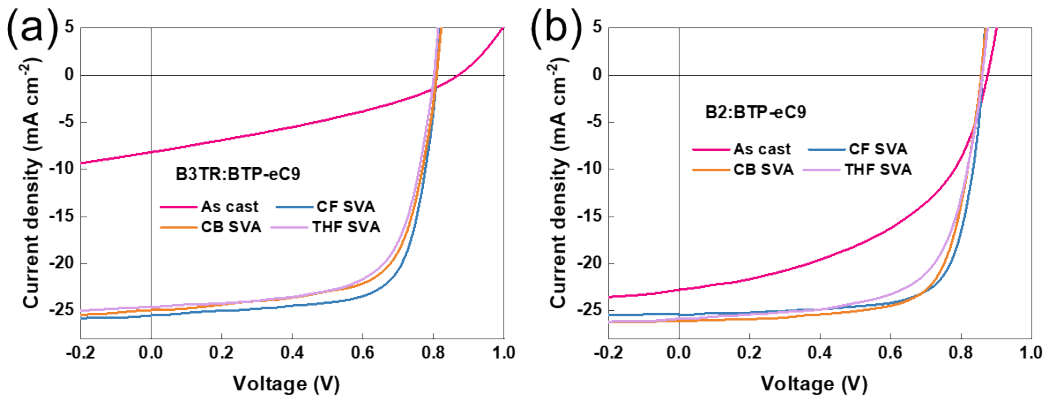

Figure S8. *J-V* curves of (a) B3TR: :BTP-eC9- and (b) B2:BTP-eC9-based cells for various SVA solvent.

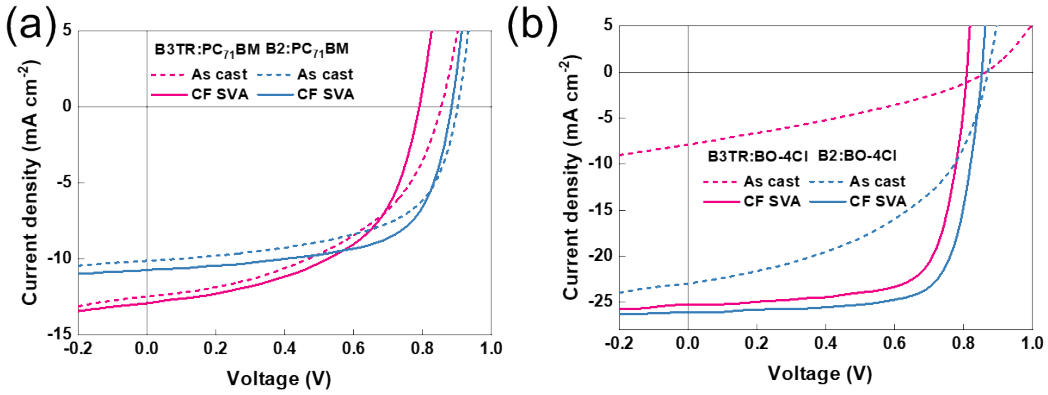

Figure S9. *J-V* curves of as-cast and CF SVA (a) B3TR:$PC_{71}BM$, B2:$PC_{71}BM$ and (b) B3TR:BO-4Cl, B2:BO-4Cl based cells.

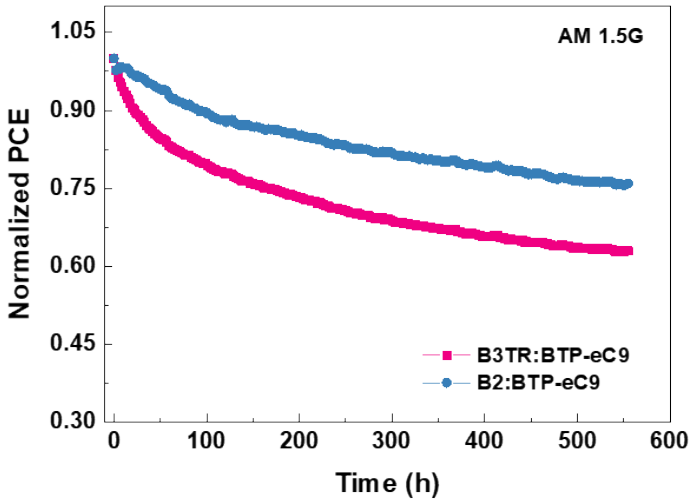

Figure S10. The stabilities of both SM-OSCs under light irradiation (simulated one-sun intensity using a LED array)

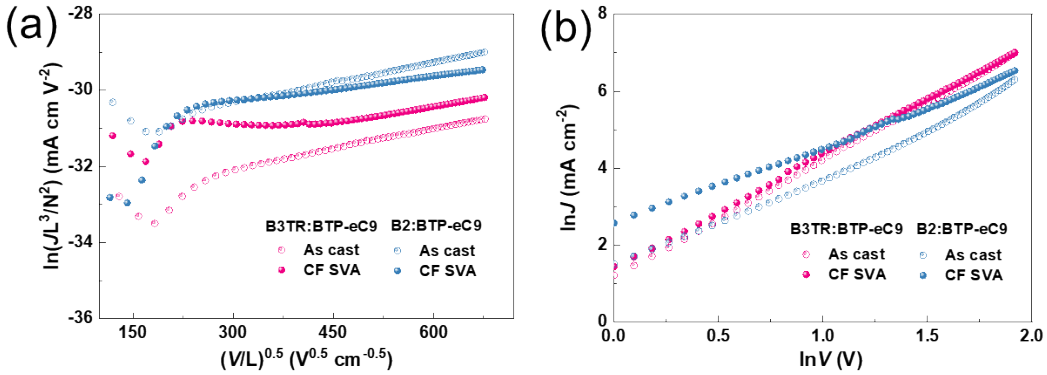

Figure S11. The hole and electron mobilities of B3TR:BTP-eC9 and B2:BTP-eC9.

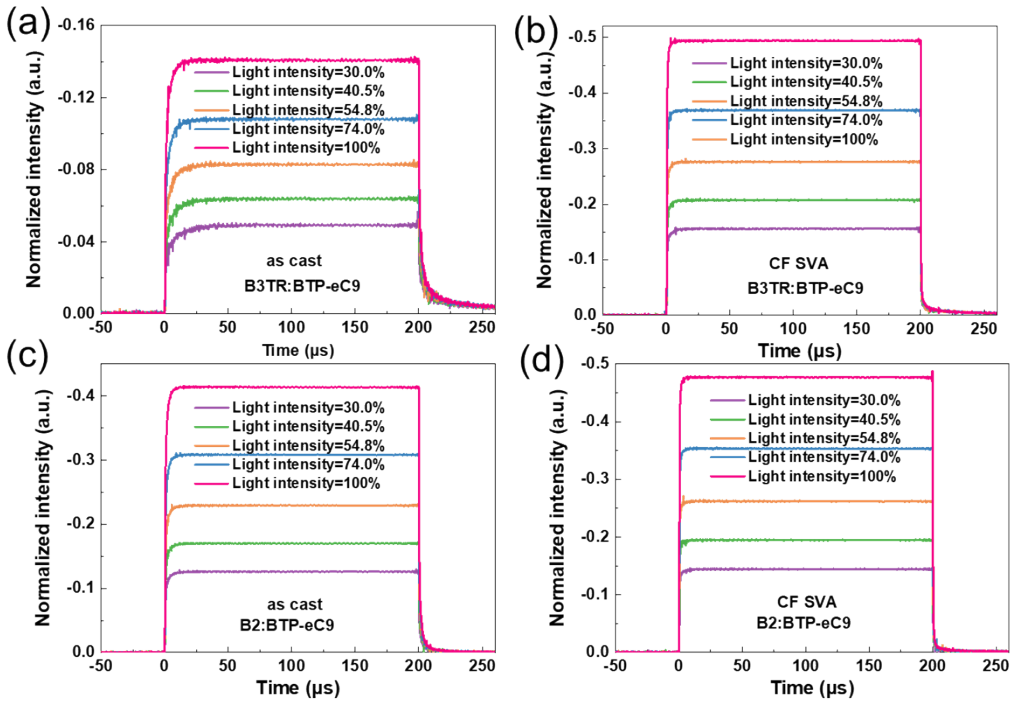

Figure S12. Transient short-circuit photocurrent of the (a,c) as cast and (b,d) CF SVA B3TR:BTP-eC9- and B2:BTP-eC9 based cells with different light intensity.

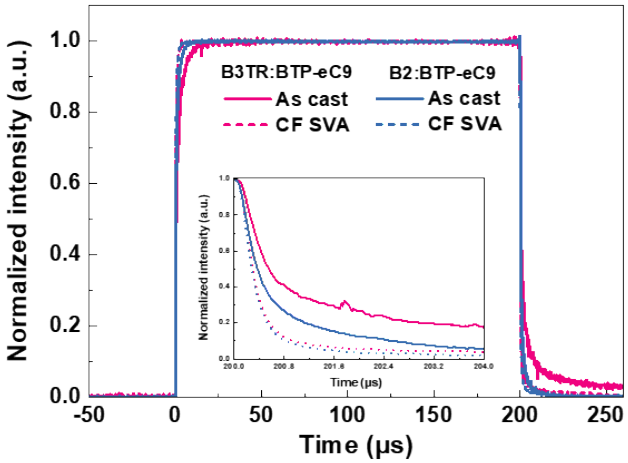

Figure S13. Normalized transient short-circuit photocurrent for as cast and CF SVA B3TR:BTP-eC9 and B2:BTP-eC9-based cells.

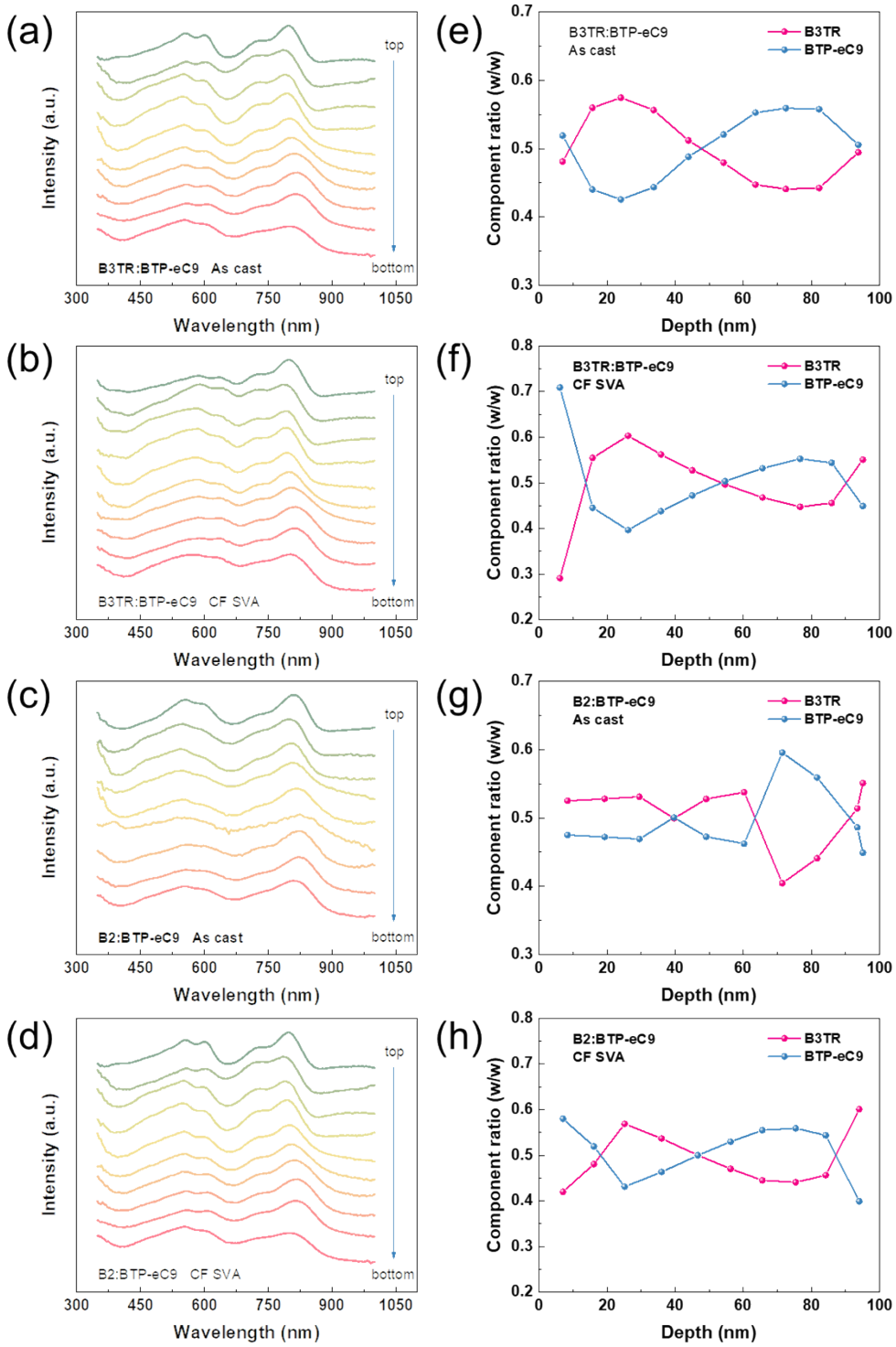

Figure S14. Film-depth-dependent optical investigations of blend films. Absorption spectra of sublayers of (a-d) B3TR:BTP-eC9 and B2:BTP-eC9 before and after CF SVA. (e-h) Vertical composition profiles as extracted from FLAS spectra of the blend films.

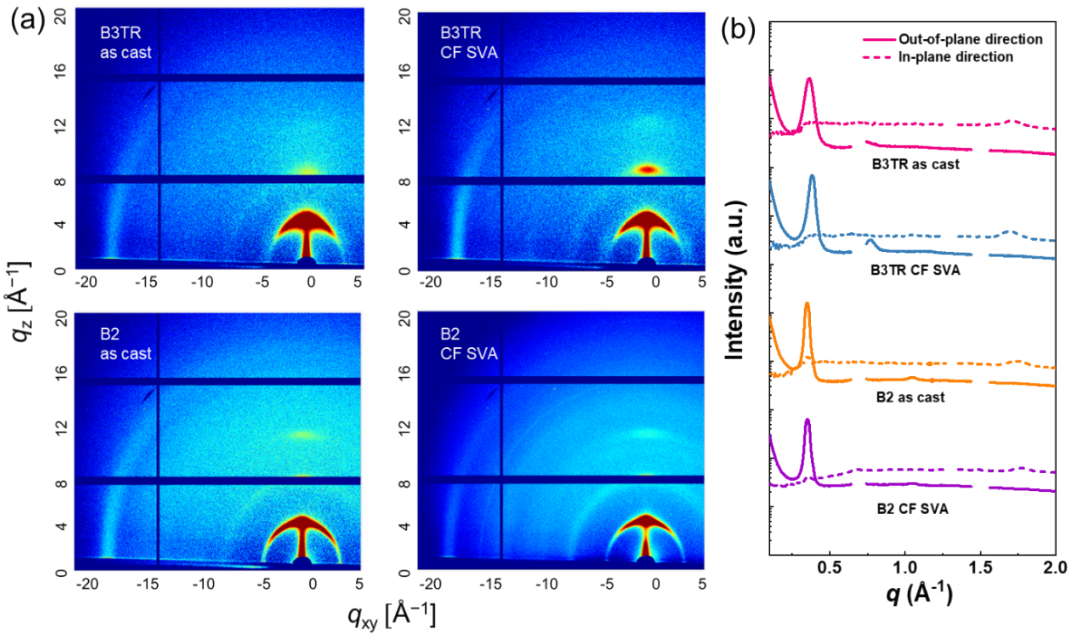

Figure S15. (a) 2D-GIWAXS patterns of as cast and CF SVA B3TR and B2 films. (b) The 1D GIWAXS profiles of as cast and CF SVA B3TR and B2 films in IP and OOP directions.

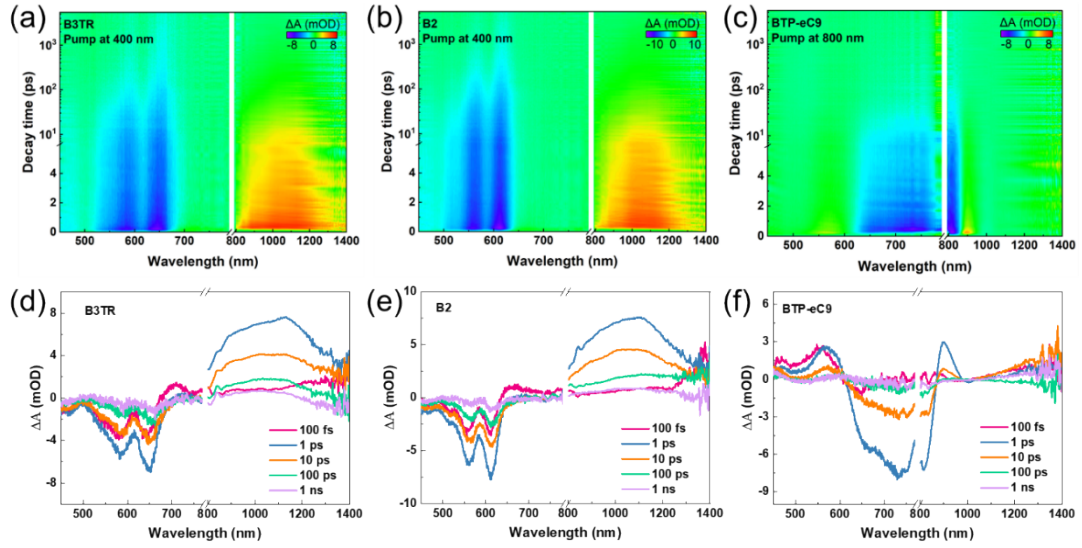

Figure S16. The TA images and the corresponding TA spectra with various decay times of the neat films with 400 or 800 nm excitation wavelength.

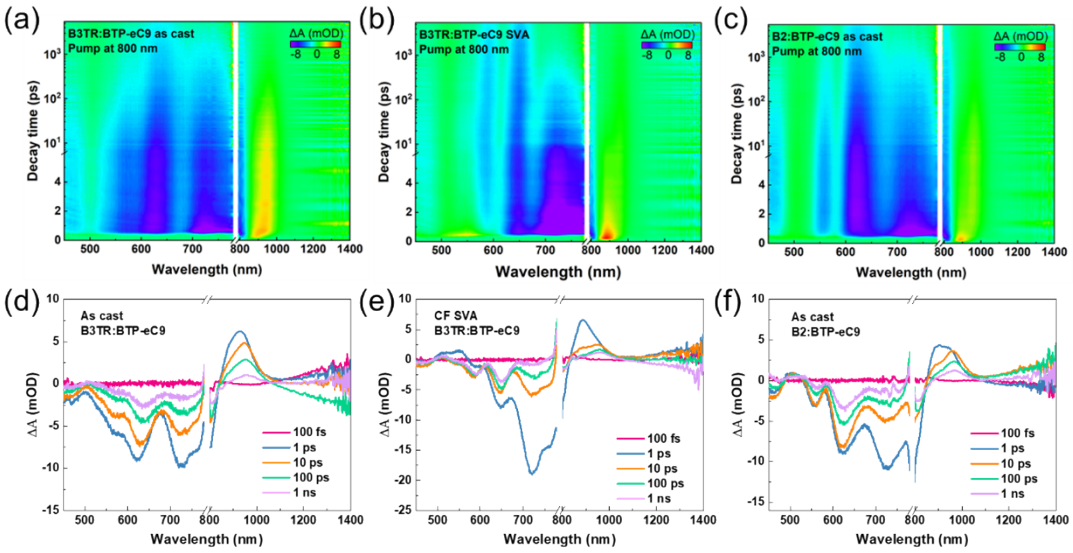

Figure S17. The TA images and the corresponding TA spectra with various decay times of the blend films with an excitation wavelength of 800 nm.

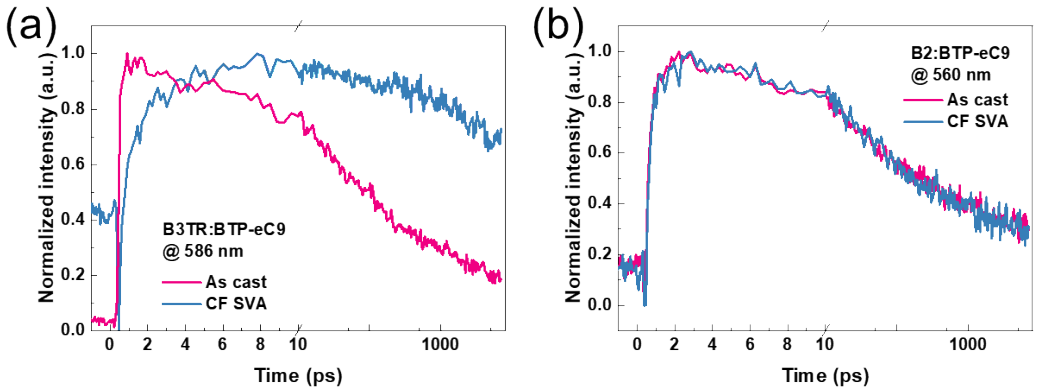

Figure S18. The decay dynamics of the TA signals at 586 and 560 nm for the (a) B3TR:BTP-eC9 and (b) B2:BTP-eC9 blend films with and without CF SVA.

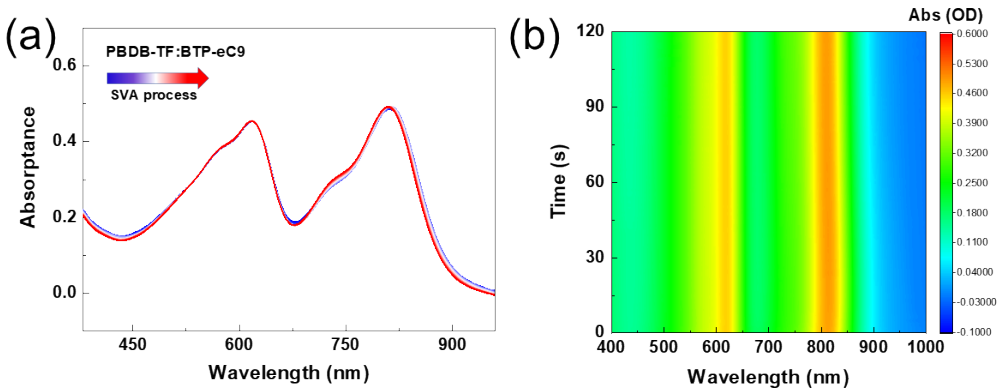

Figure S19. (a) In situ UV-visible absorption spectra and (b) in situ 2D UV-visible absorption profile of PBDB-TF:BTP-eC9 during CF SVA process.

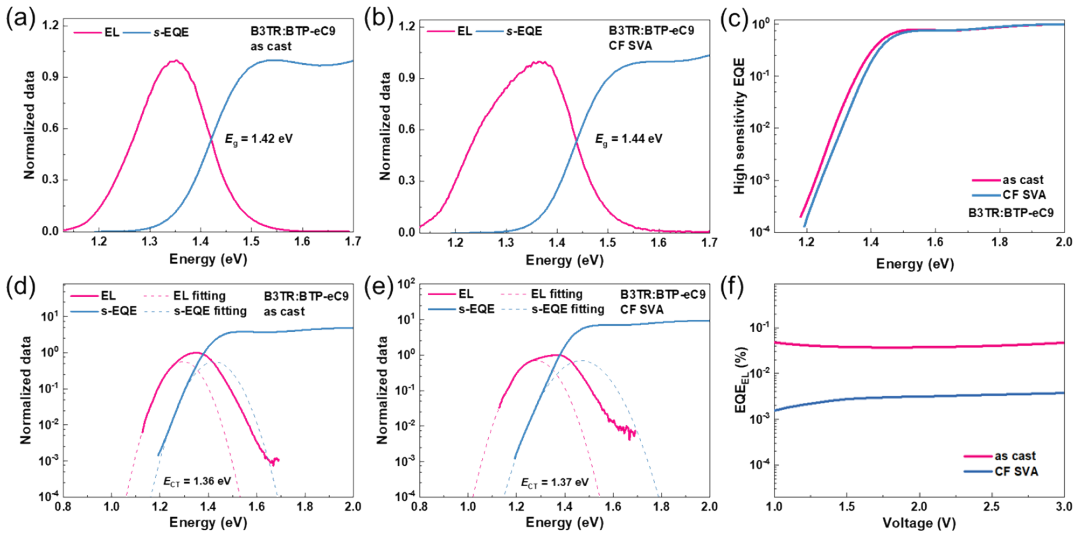

Figure S20. Normalized EL counts and normalized s-EQE curves of (a) as cast and (b) CF SVA B3TR:BTP-eC9 for determining bandgaps. (c) Highly sensitive EQE curves of as cast and CF SVA B3TR:BTP-eC9. Reduced EL and s-EQE and their fitted curves of (d) as cast and (e) CF SVA B3TR:BTP-eC9. (f) EQE_{EL} curves of as cast and CF SVA B3TR:BTP-eC9.

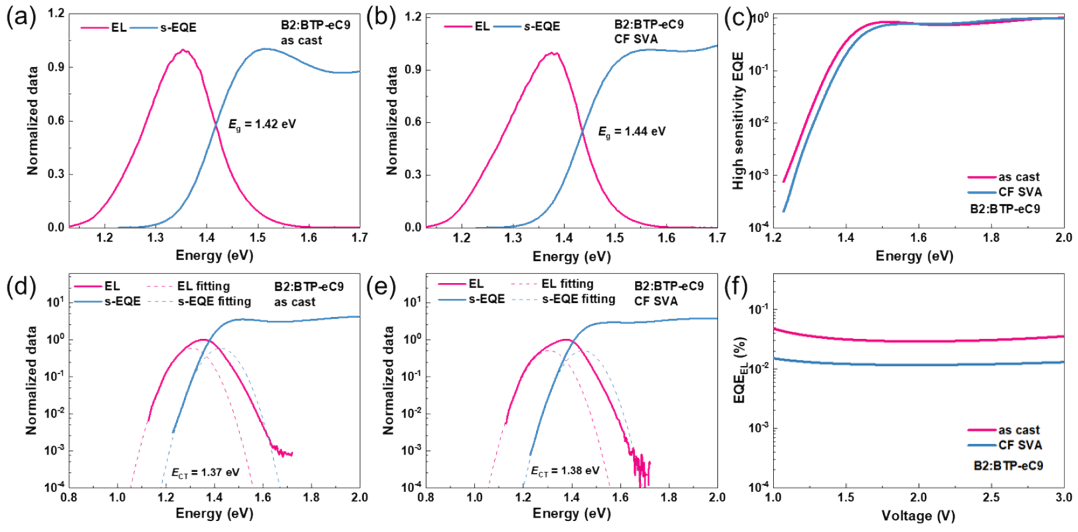

Figure S21. Normalized EL counts and normalized s-EQE curves of (a) as cast and (b) CF SVA B2:BTP-eC9 for determining bandgaps. (c) Highly sensitive EQE curves of as cast and CF SVA B2:BTP-eC9. Reduced EL and s-EQE and their fitted curves of (d) as cast and (e) CF SVA B2:BTP-eC9. (f) EQE_{EL} curves of as cast and CF SVA B2:BTP-eC9.

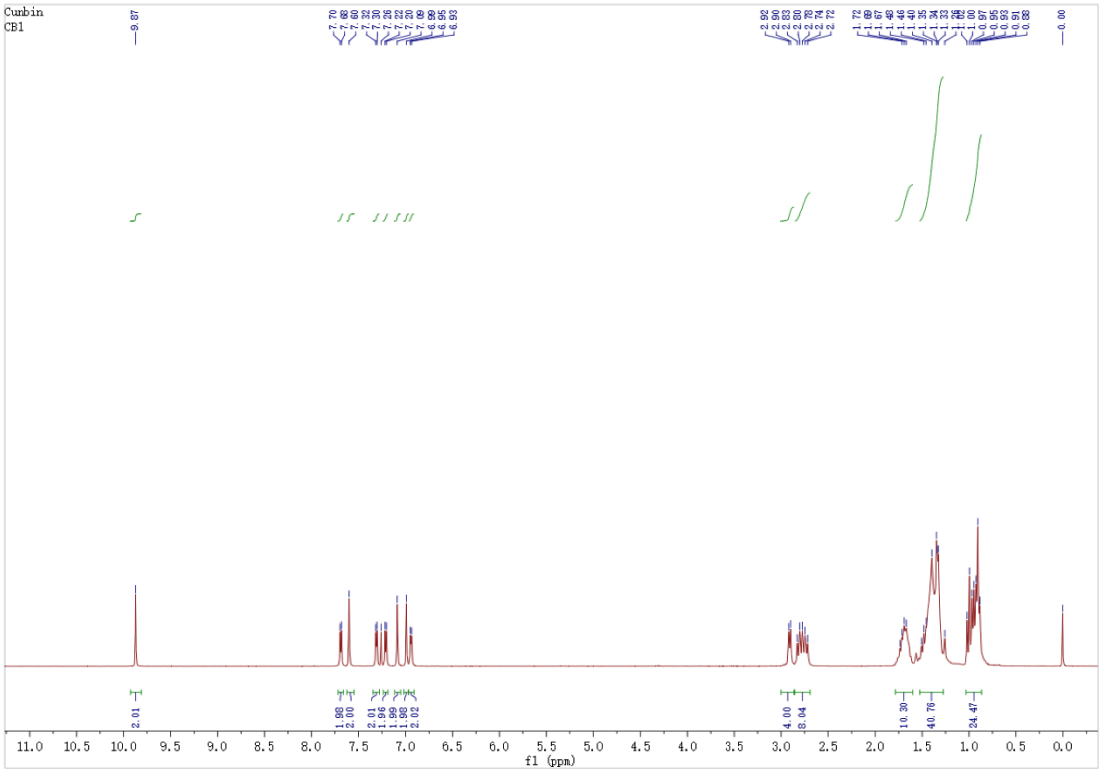

Figure S22. The ^{1}H-NMR spectrum of **S3** in $CDCl_3$.

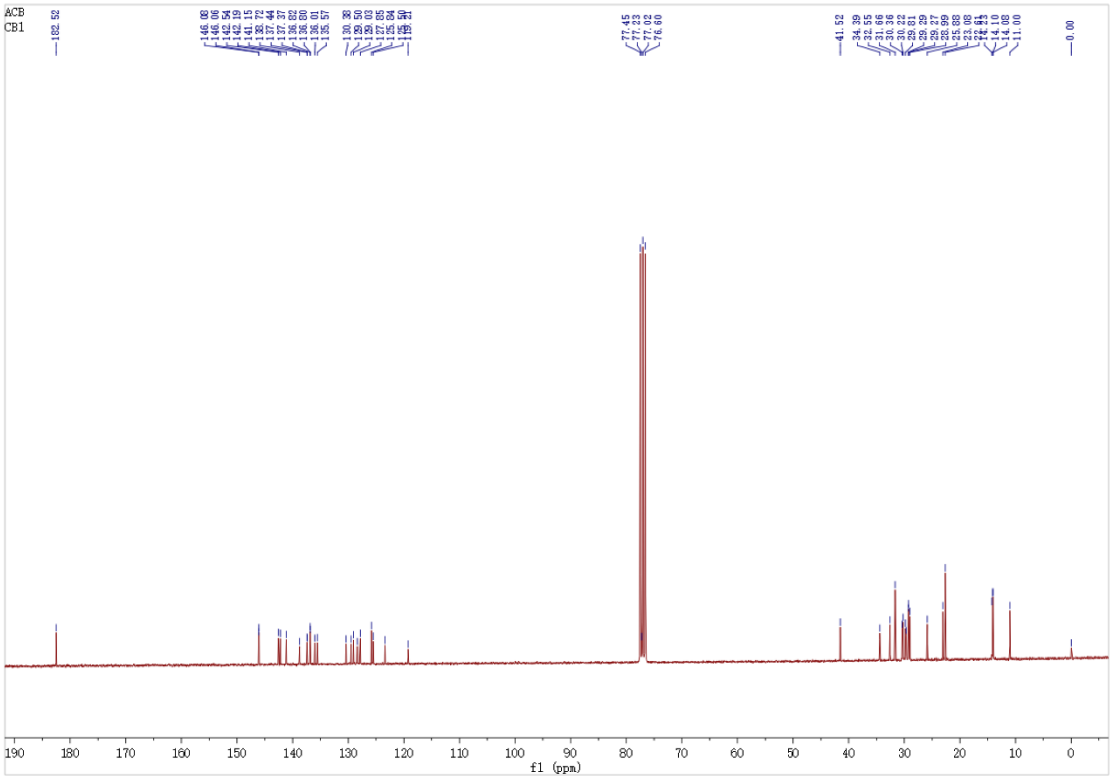

Figure S23. The ^{13}C-NMR spectrum of **S3** in $CDCl_3$.

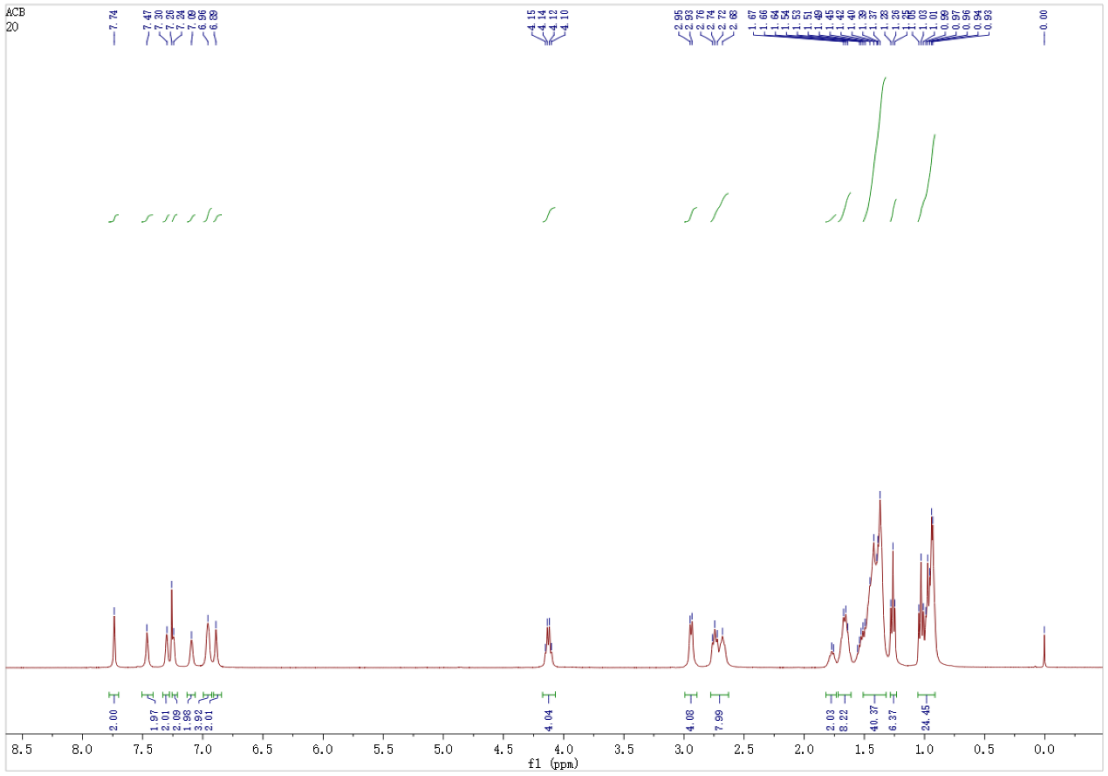

Figure S24. The ^{1}H-NMR spectrum of **B3TR** in $CDCl_3$.

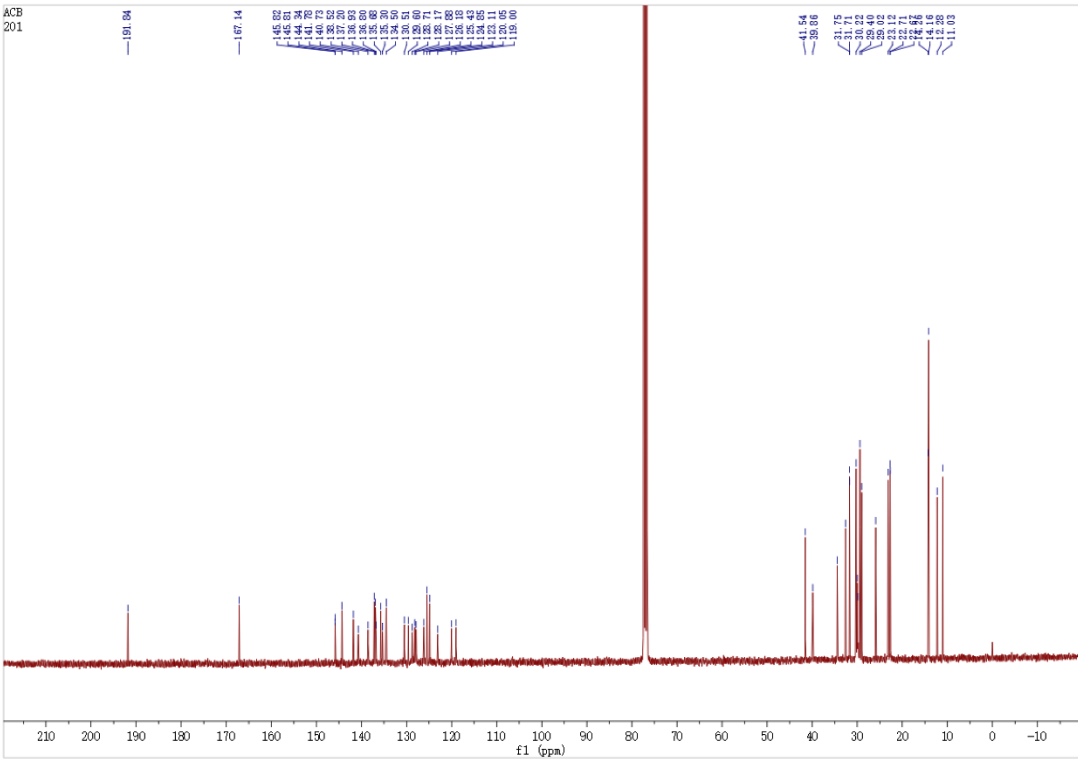

Figure S25. The ^{13}C-NMR spectrum of **B3TR** in $CDCl_3$.

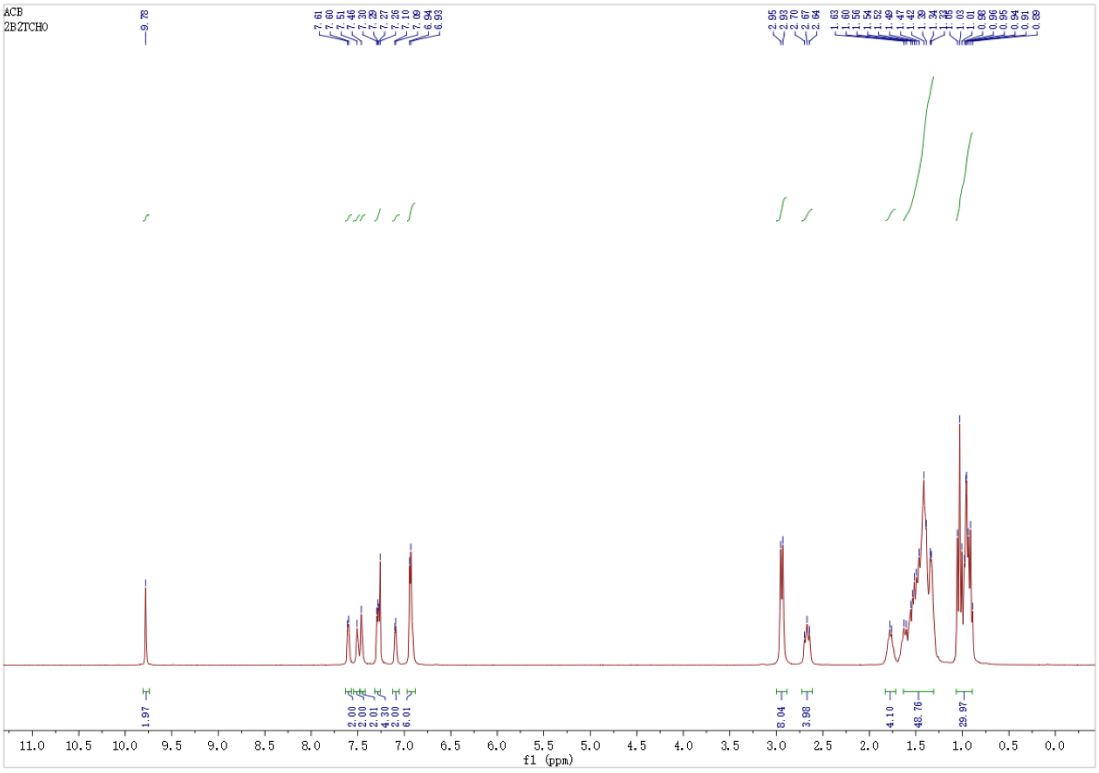

Figure S26. The ^{1}H-NMR spectrum of **S7** in $CDCl_3$.

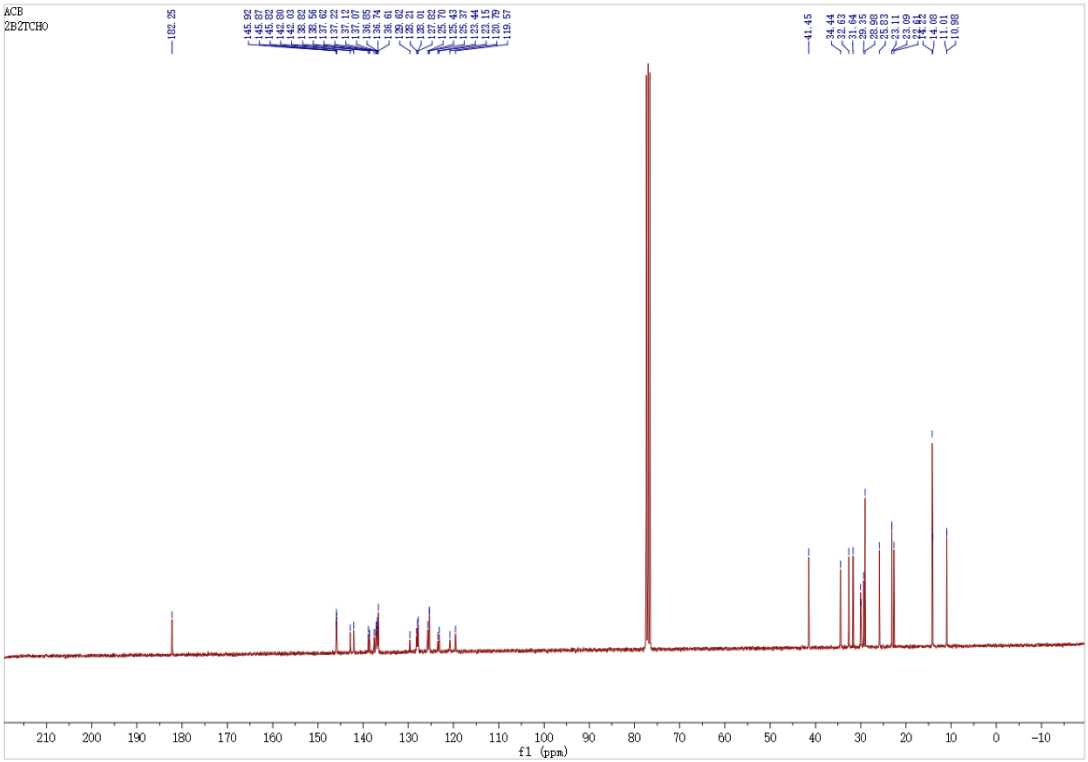

Figure S27. The ^{13}C-NMR spectrum of **S7** in $CDCl_3$.

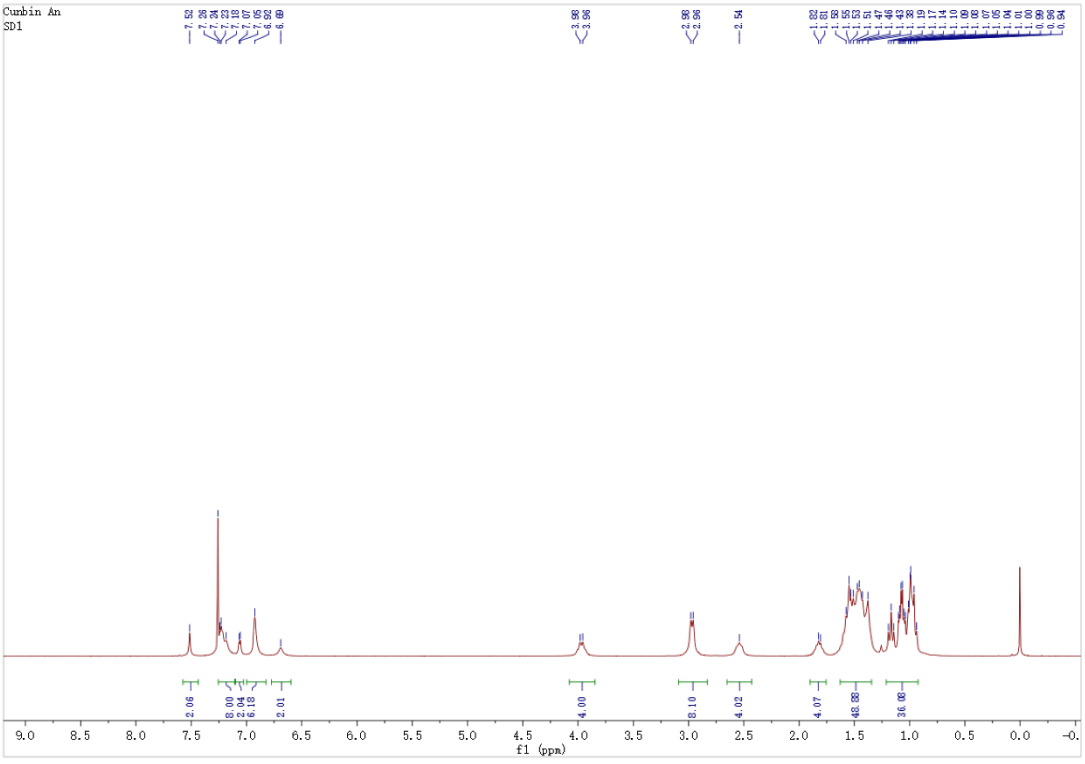

Figure S28. The ^{1}H-NMR spectrum of **B2** in $CDCl_3$.

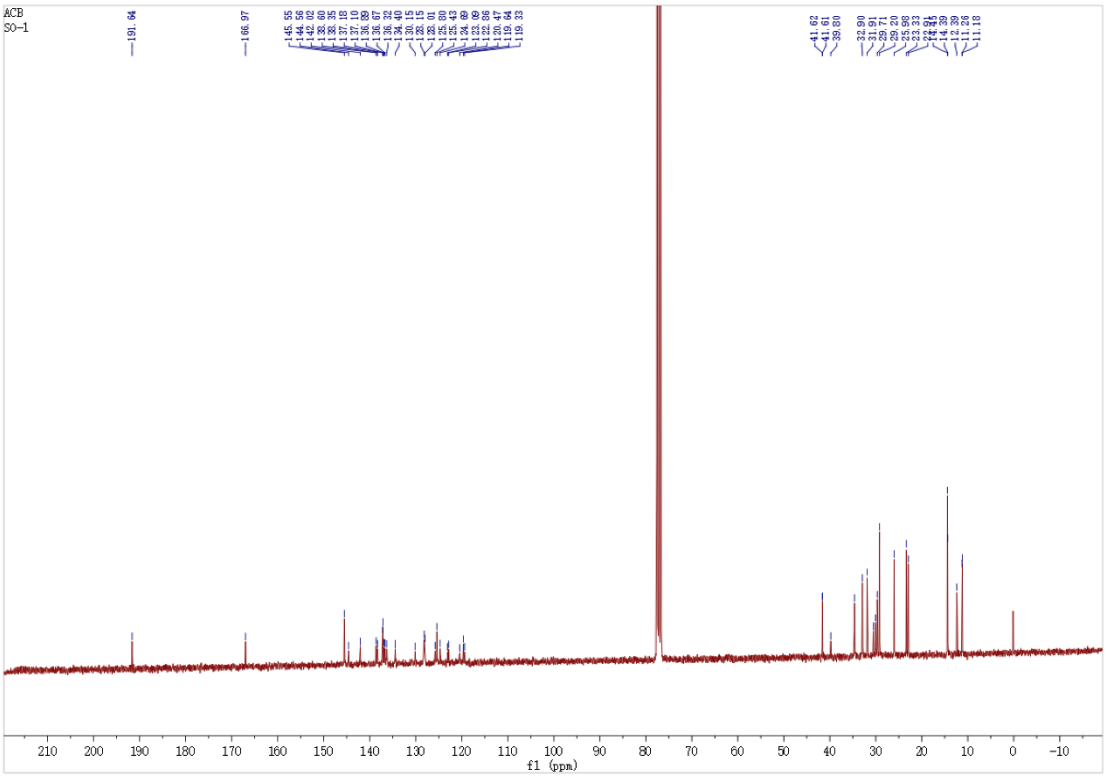

Figure S29. The ^{13}C-NMR spectrum of **B2** in $CDCl_3$.

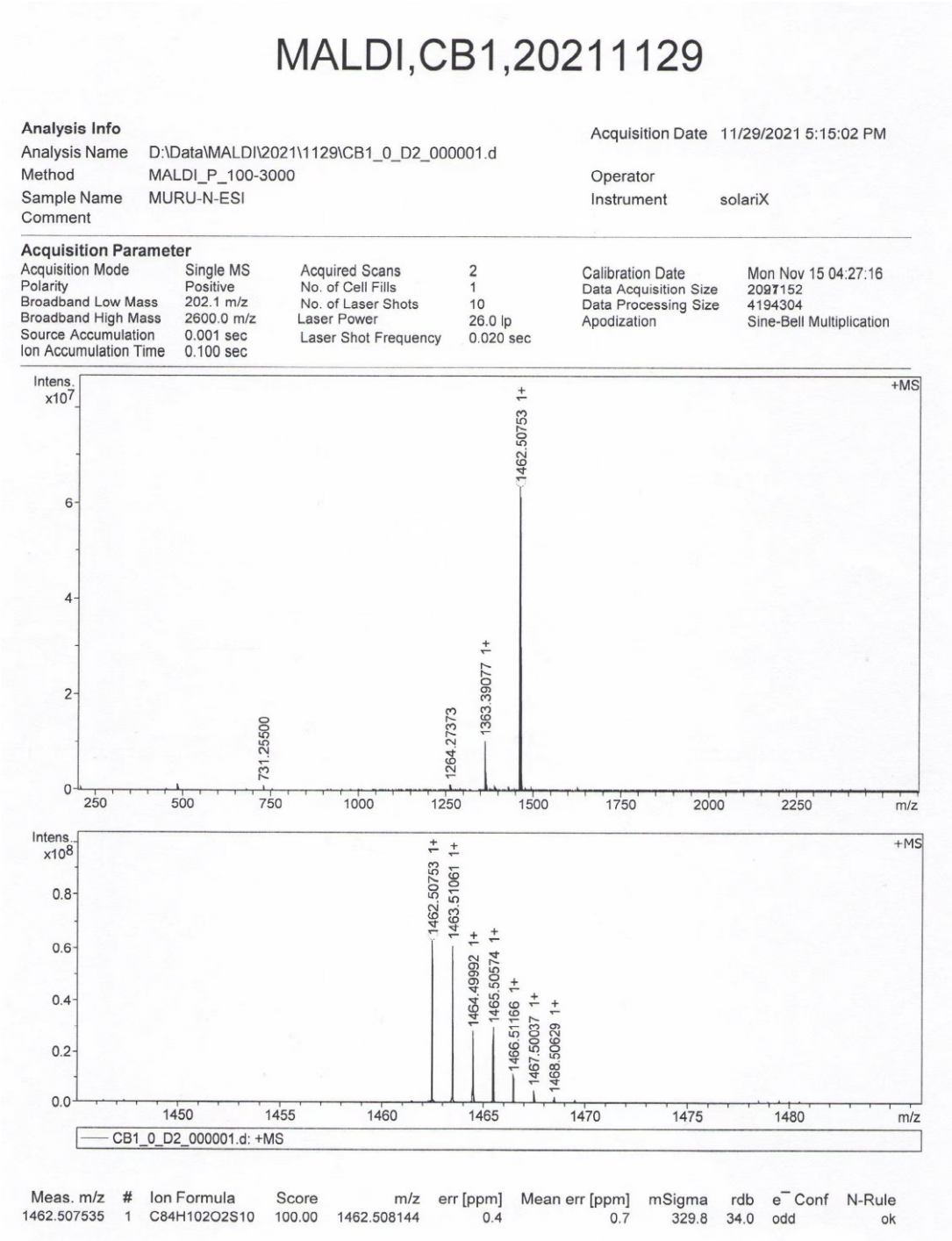

Figure S30. The HRMS spectrum of **S3**.

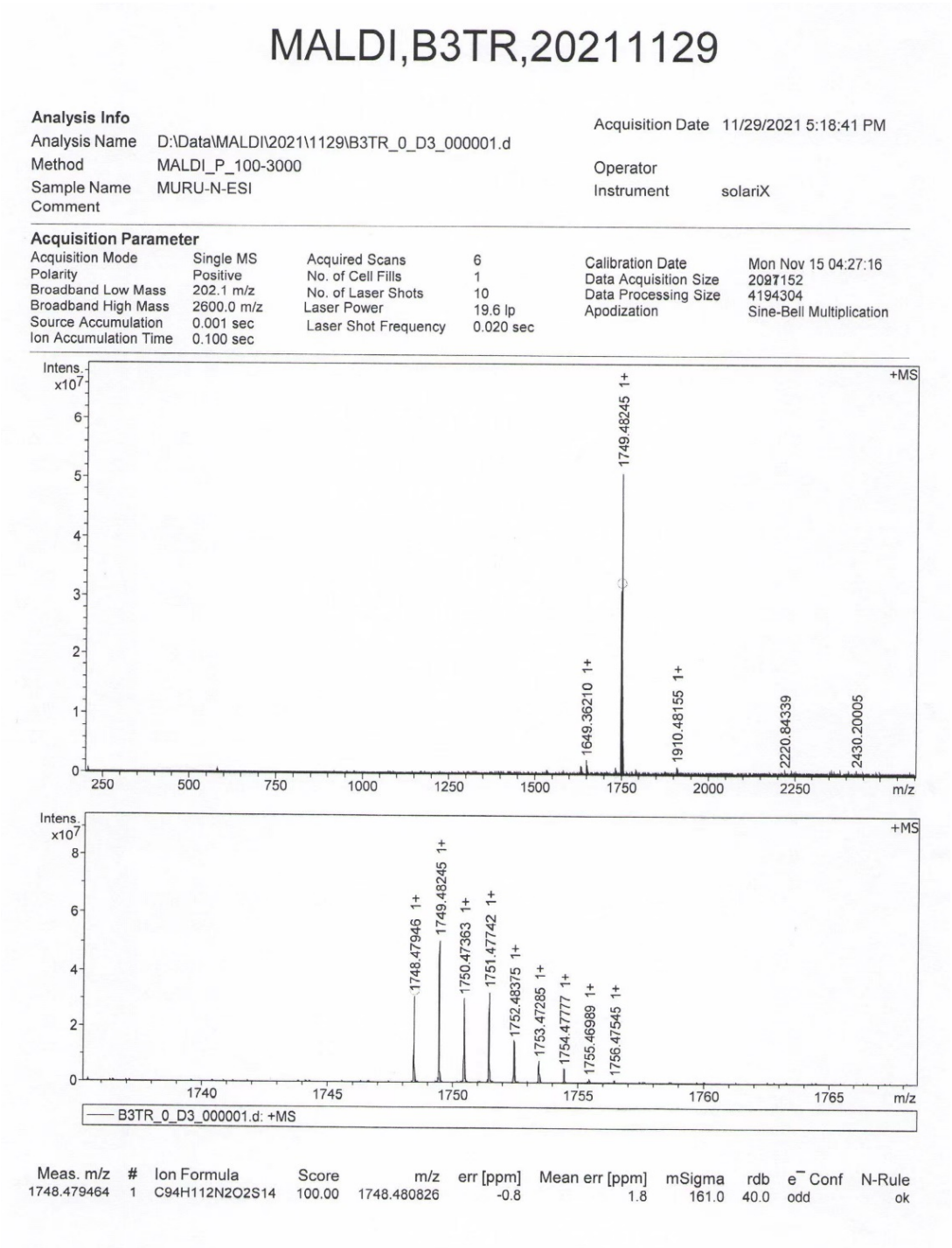

Figure S31. The HRMS spectrum of **B3TR**.

MALDI,CHO,20240119

Analysis Info

Analysis Name	D:\Data\MALDI\2021\0818\CHO_0_G8_000004.d	Acquisition Date	8/18/2021 4:48:49 PM
Method	MALDI_P_100-3000	Operator	
Sample Name	MURU-N-ESI	Instrument	solariX
Comment			

Acquisition Parameter

Acquisition Mode	Single MS	Acquired Scans	3	Calibration Date	Mon Aug 16 04:41:45
Polarity	Positive	No. of Cell Fills	1	Data Acquisition Size	2097152
Broadband Low Mass	202.1 m/z	No. of Laser Shots	10	Data Processing Size	4194304
Broadband High Mass	2600.0 m/z	Laser Power	59.4 lp	Apodization	Sine-Bell Multiplication
Source Accumulation	0.001 sec	Laser Shot Frequency	0.020 sec		
Ion Accumulation Time	0.100 sec				

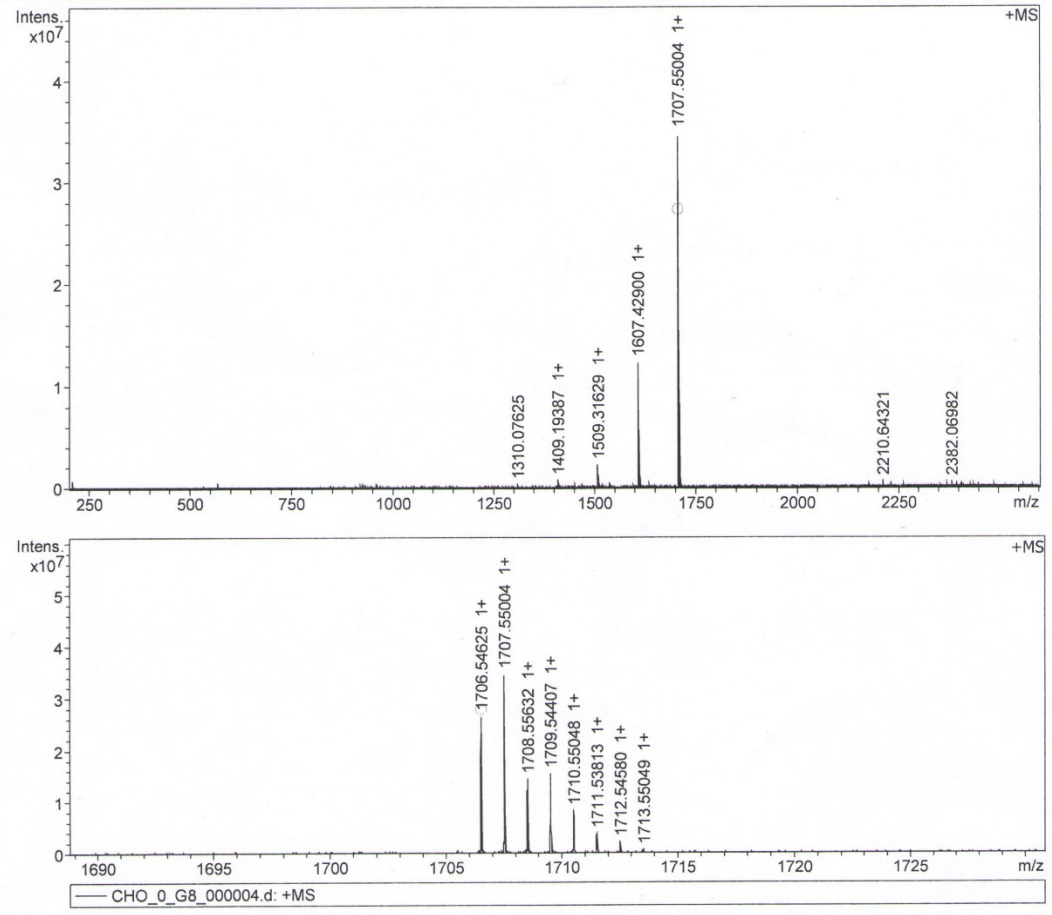

Meas. m/z	#	Ion Formula	Score	m/z	err [ppm]	Mean err [ppm]	mSigma	rdb	e⁻ Conf	N-Rule
1706.546254	1	C98H114O2S12	100.00	1706.546186	0.0	0.8	240.4	42.0	odd	ok

Figure S32. The HRMS spectrum of **S7**.

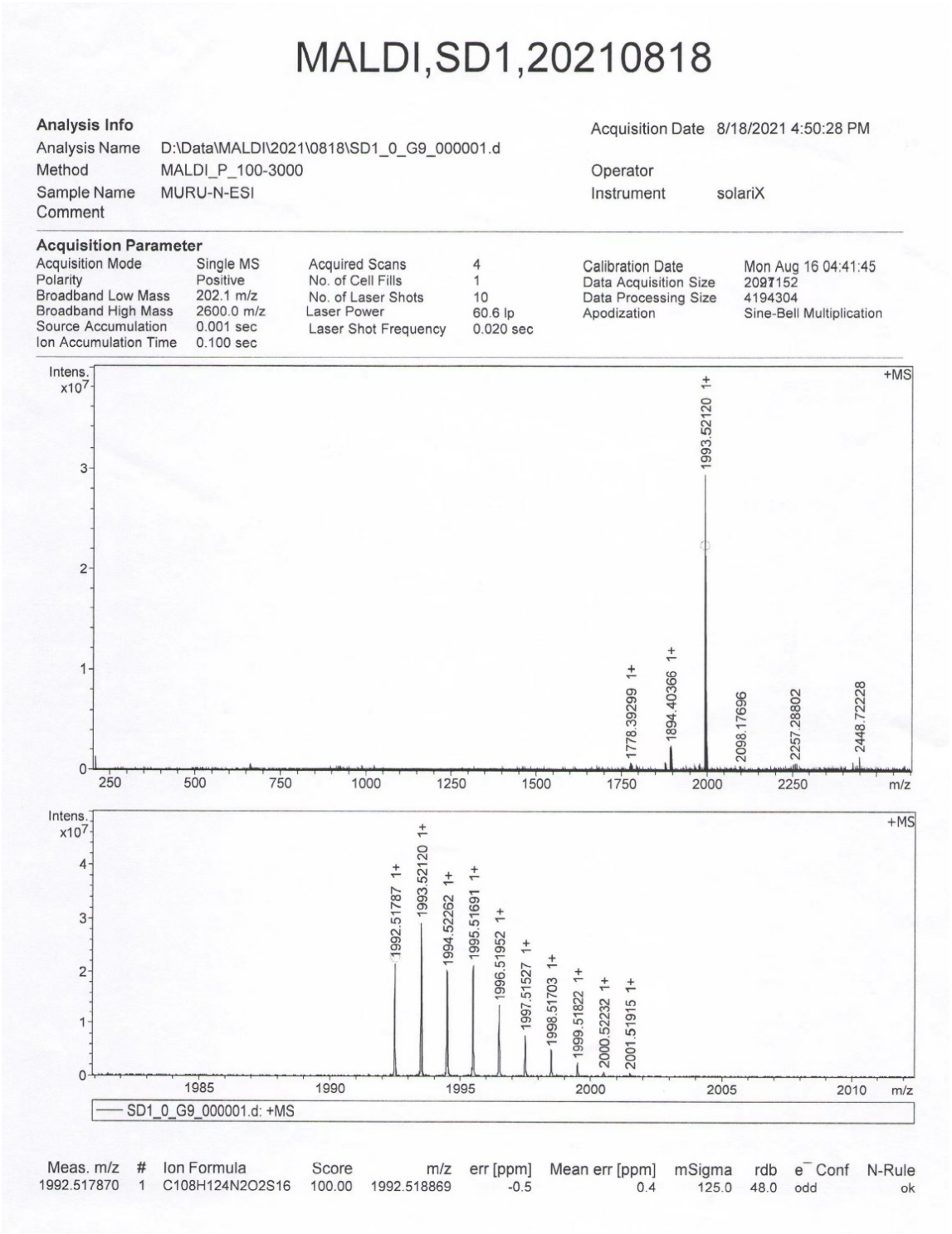

Figure S33. The HRMS spectrum of **B2**.

Table S1. The detailed parameter of B3TR:BTP-eC9-based cells for different CF SVA duration under simulated AM 1.5G (100 mW cm^{-2}) illumination.

SVA time	V_{OC} (V)	J_{SC} (mA cm^{-2})	FF	PCE (%) [a)]
0	0.870	8.16	0.332	2.36
40s	0.818	24.9	0.471	9.58
50s	0.807	25.7	0.482	10.1
60s	0.800	25.5	0.646	13.2
70s	0.809	25.5	0.720	14.8
80s	0.808	25.3	0.723	14.8

Table S2. The detailed parameter of B2:BTP-eC9-based cells for different CF SVA duration under simulated AM 1.5G (100 mW cm^{-2}) illumination.

SVA time	V_{OC} (V)	J_{SC} (mA cm^{-2})	FF	PCE (%) [a)]
0	0.876	22.8	0.491	9.80
40s	0.866	25.7	0.512	11.4
50s	0.863	25.9	0.570	12.8
60s	0.862	26.4	0.735	16.7
70s	0.861	26.2	0.758	17.1
80s	0.860	26.1	0.706	15.9

Table S3. The detailed parameter of B3TR:BTP-eC9-based cells for various SVA solvent under simulated AM 1.5G (100 mW cm^{-2}) illumination.

Treatment	V_{OC} (V)	J_{SC} (mA cm^{-2})	FF	PCE (%) [a)]
As cast	0.870	8.16	0.332	2.36
CF SVA	0.809	25.5	0.720	14.8
CB SVA	0.808	24.9	0.683	13.8
THF SVA	0.802	24.6	0.676	13.4

Table S4. The detailed parameter of B2:BTP-eC9-based cells for various SVA solvent under simulated

AM 1.5G (100 mW cm^{-2}) illumination.

Treatment	V_{OC} (V)	J_{SC} (mA cm^{-2})	FF	PCE (%) [a)]
As cast	0.876	22.8	0.491	9.80
CF SVA	0.861	26.2	0.758	17.1
CB SVA	0.857	26.1	0.722	16.1
THF SVA	0.861	25.8	0.669	14.9

Table S5. The detailed parameter of different ASM-OSCs for different treatment under simulated AM 1.5G (100 mW cm^{-2}) illumination.

Active layers	**Treatment**	**V_{OC} (V)**	**J_{SC} (mA cm^{-2})**	**FF**	**PCE (%)**	**Reference**
BTR:	As cast	0.96	11.64	0.47	5.2	[1]
$PC_{71}BM$	THF SVA	0.90	13.9	0.74	9.3	
RCN5T:	As cast	0.99	7.09	0.50	3.51	[2]
$PC_{71}BM$	TA+SVA	0.92	15.88	0.69	10.08	
DRIB-T-C4:IT-4F	As cast	1.00	10.59	0.31	3.29	[3]
	THF SVA	0.930	18.34	0.65	11.14	
ZnP-TBO:6ITC	As cast	0.84	14.92	0.489	6.00	[4]
	DIO+SVA	0.80	20.44	0.739	12.08	
ZR2-C3:Y6	As cast	0.898	13.93	0.346	4.33	[5]
	120℃ TA	0.854	24.70	0.701	14.78	
BSCl: IDIC-4Cl	As cast	0.900	7.7	33.9	2.35	[6]
	TA+SVA	0.865	21.5	70.9	13.03	

Table S6. The detailed parameter of B3TR: PC71BM- and B2:PC71BM-based cells under simulated AM 1.5G (100 mW cm-2) illumination.

Active layer	Treatment	V_{OC} (V)	J_{SC} (mA cm^{-2})	FF	PCE (%) [a)]
B3TR:$PC_{71}BM$	As-cast	0.854	12.5	0.475	5.07
	CF SVA	0.790	12.9	0.531	5.41
B2:$PC_{71}BM$	As-cast	0.901	10.1	0.588	5.35
	CF SVA	0.884	10.7	0.639	6.04

Table S7. The detailed parameter of B3TR:BO-4Cl- and B2: BO-4Cl-based cells under simulated AM 1.5G (100 mW cm^{-2}) illumination.

Active layer	Treatment	V_{OC} (V)	J_{SC} (mA cm^{-2})	FF	PCE (%) [a)]
B3TR:BO-4Cl	As-cast	0.865	7.86	0.326	2.21
	CF SVA	0.808	25.3	0.723	14.8
B2:BO-4Cl	As-cast	0.870	23.0	0.479	9.60
	CF SVA	0.853	26.1	0.742	16.5

[1] K. Sun, Z. Xiao, S. Lu, W. Zajaczkowski, W. Pisula, E. Hanssen, J. M. White, R. M. Williamson, J. Subbiah, J. Ouyang, A. B. Holmes, W. W. H. Wong, D. J. Jones, Nat. Commun. 2015, 6, 6013.

[2] B. Kan, M. Li, Q. Zhang, F. Liu, X. Wan, Y. Wang, W. Ni, G. Long, X. Yang, H. Feng, Y. Zuo, M. Zhang, F. Huang, Y. Cao, T. P. Russell, Y. Chen, J. Am. Chem. Soc. 2015, 137, 3886-3893.

[3] L. Yang, S. Zhang, C. He, J. Zhang, Y. Yang, J. Zhu, Y. Cui, W. Zhao, H. Zhang, Y. Zhang, Z. Wei, J. Hou, Chem. Mater. 2018, 30, 2129-2134.

[4] K. Gao, S. B. Jo, X. Shi, L. Nian, M. Zhang, Y. Kan, F. Lin, B. Kan, B. Xu, Q. Rong, L. Shui, F. Liu, X. Peng, G. Zhou, Y. Cao, A. K.-Y. Jen, Adv. Mater. 2019, 31, 1807842.

[5] R. Zhou, Z. Jiang, Y. Shi, Q. Wu, C. Yang, J. Zhang, K. Lu, Z. Wei, Adv. Funct. Mater. 2020, 30, 2005426.

[6] Z. Zhang, Q. Wu, D. Deng, S. Wu, R. Sun, J. Min, J. Zhang, Z. Wei, J. Mater. Chem. C 2020, 8, 15385-15392.